A&A 577, A39 (2015)
DOI: 10.1051/0004-6361/201525719

Astronomy & Astrophysics

No trace of a single-degenerate companion in late spectra of supernovae 2011fe and 2014J

P. Lundqvist[1], A. Nyholm[1], F. Taddia[1], J. Sollerman[1], J. Johansson[2], C. Kozma[1], N. Lundqvist[1], C. Fransson[1], P. M. Garnavich[3], M. Kromer[1], B. J. Shappee[4], and A. Goobar[2]

[1] Department of Astronomy and The Oskar Klein Centre, AlbaNova University Center, Stockholm University, 106 91 Stockholm, Sweden
e-mail: peter@astro.su.se
[2] Physics Department and The Oskar Klein Centre, AlbaNova University Center, Stockholm University, 106 91 Stockholm, Sweden
[3] 225 Nieuwland Science, University of Notre Dame, Notre Dame, IN 46556-5670, USA
[4] Carnegie Observatories, 813 Santa Barbara Street, Pasadena, CA 91101, USA

Received 22 January 2015 / Accepted 22 February 2015

ABSTRACT

Aims. This study aims at constraining the origin of the nearby Type Ia supernovae (SNe), 2011fe and 2014J. The two most favoured scenarios for triggering the explosion of the white dwarf supernova progenitor is either mass loss from a non-degenerate companion or merger with another white dwarf. In the former, there could be a significant amount of leftover material from the companion at the centre of the supernova. Detecting such material would therefore favour the single-degenerate scenario.
Methods. The left-over material from a possible non-degenerate companion can reveal itself after about one year, and in this study such material was searched for in the spectra of SN 2011fe (at 294 days after the explosion) using the Large Binocular Telescope and for SN 2014J using the Nordic Optical Telescope (315 days past explosion). The observations were interpreted using numerical models simulating the expected line emission from ablated material from the companion star. The spectral lines sought for are Hα, [O I] λ6300, and [Ca II] $\lambda\lambda$7291,7324, and the expected width of these lines is $\sim$1000 km s^{-1}, which in the case of the [Ca II] lines blend to a broader feature.
Results. No signs of Hα, [O I] λ6300, or [Ca II] $\lambda\lambda$7291, 7324 could be traced for in any of the two supernovae. When systematic uncertainties are included, the limits on hydrogen-rich ablated gas are 0.003 $M_\odot$ in SN 2011fe and 0.0085 $M_\odot$ in SN 2014J, where the limit for SN 2014J is the second lowest ever, and the limit for SN 2011fe is a revision of a previous limit. Limits are also put on helium-rich ablated gas, and here limits from [O I] λ6300 provide the upper mass limits 0.002 $M_\odot$ and 0.005 $M_\odot$ for SNe 2011fe and 2014J, respectively. These numbers are used in conjunction with other data to argue that these supernovae can stem from double-degenerate systems or from single-degenerate systems with a spun-up/spun-down super-Chandrasekhar white dwarf. For SN 2011fe, other types of hydrogen-rich donors can very likely be ruled out, whereas a main-sequence donor system with large intrinsic separation is still possible for SN 2014J. Helium-rich donor systems cannot be ruled out for any of the two supernovae, but the expected short delay time for such progenitors makes this possibility less likely, especially for SN 2011fe. Published data for SNe 1998bu, 2000cx, 2001el, 2005am, and 2005cf are used to constrain their origin. We emphasise that the results of this study depend on the sought-after lines emerging unattenuated from the central regions of the nebula. Detailed radiative transfer calculations with longer line lists than are presently used are needed to confirm that this is, in fact, true. Finally, the broad lines of SNe 2011fe and 2014J are discussed, and it is found that the [Ni II] λ7378 emission is redshifted by $\sim$+1300 km s^{-1}, as opposed to the known blueshift of $\sim$−1100 km s^{-1} for SN 2011fe. [Fe II] λ7155 is also redshifted in SN 2014J. SN 2014J belongs to a minority of SNe Ia that both have a nebular redshift of [Fe II] λ7155 and [Ni II] λ7378, and a slow decline of the Si II λ6355 absorption trough just after B-band maximum.

Key words. supernovae: general – supernovae: individual: SN 2011fe – supernovae: individual: SN 2014J

1. Introduction

It is widely thought that a Type Ia supernova (SN Ia) is the thermonuclear explosion of a carbon/oxygen white dwarf (WD). The two most common scenarios are that the explosion could be triggered by mass transfer from a non-compact companion star (the single-degenerate scenario: Whelan & Iben 1973; Nomoto 1982) or that it is the result of a merger with another WD (the double-degenerate scenario: Whelan & Iben 1973; Iben & Tutukov 1984; Webbink 1984). While the single-degenerate (SD) scenario where a WD at the Chandrasekhar limit accretes matter from a close companion has been the most favoured one, there is now growing evidence that the double-degenerate (DD) scenario could be the dominant channel for SNe Ia (e.g., Maoz et al. 2014).

The lack of knowledge about the true nature of the progenitor systems of SNe Ia is a big disadvantage, since they are used as standardisable candles for distance determinations in cosmology (e.g., Goobar & Leibundgut 2011) and were used to discover the accelerating expansion of the Universe (e.g., Riess et al. 1998; Perlmutter et al. 1999). To do precision cosmology, systematic effects related to the type of progenitor system should be minimised, and possibilities of identifying the nature and origin of these systems must be probed.

One way to constrain the nature of the progenitor systems is to look for merger left over from the companion star in SD scenarios. This could either be done by searching for absorption or emission lines from a circumstellar medium (CSM) around normal SNe Ia (e.g., Mattila et al. 2005; Patat et al. 2007b;

Simon et al. 2009; Dilday et al. 2012; Lundqvist et al. 2013; Sternberg et al. 2014) or by identifying material blasted off or evaporated from the non-compact companion owing to the impact of the SN ejecta (e.g., Mattila et al. 2005; Leonard 2007; Shappee et al. 2013; Lundqvist et al. 2013; Maeda et al. 2014). Of these, absorption lines from a CSM may be the least conclusive, since such lines may also exist in DD scenarios (Shen et al. 2013) or in alternative scenarios for SNe Ia (e.g., Soker 2015).

Detecting early X-ray or radio emission due to interaction between the supernova ejecta and a CSM would argue for a SD scenario, but no such emission has ever been observed from a SN Ia (e.g., Panagia et al. 2006; Hughes et al. 2007; Hancock et al. 2011; Russell & Immler 2012), not even from the very nearby SNe 2011fe and 2014J, a fact that has been used to rule out most SD scenarios for those supernovae (Chomiuk et al. 2012; Horesh et al. 2011; Margutti et al. 2012, 2014; Pérez-Torres et al. 2014). There are, however, SD scenarios that predict a very tenuous CSM in the vicinity of the explosion (e.g., Di Stefano et al. 2011; Justham 2011; Hachisu et al. 2012), so non-detections of radio and X-ray emission from SNe Ia are not necessarily fully conclusive in terms of DD or SD scenarios.

Here we concentrate on probing possible material from a SD companion in late optical spectra of SN 2014J, the closest SN Ia for decades. We do this in the same way as previously done for six other SNe Ia (e.g., Mattila et al. 2005; Leonard 2007; Lundqvist et al. 2013; Shappee et al. 2013), including the nearby SN 2011fe. For the latter, Shappee et al. (2013) claim that an upper limit of 0.001 $M_{\odot}$ of solar-abundance material is present in the innermost ejecta of the supernova, which is in clear conflict with hydrodynamical simulations of SD scenarios (Marietta et al. 2000; Pakmor et al. 2008; Liu et al. 2012, 2013a; Pan et al. 2012). For the five other SNe Ia, the upper mass limit was 0.01–0.03 $M_{\odot}$, which is in marginal conflict with SD scenarios.

A way to avoid conflict between the lack of hydrogen lines in late spectra and hydrodynamical models is to assume that the SD companion was rich in helium. In such a case, 0.0024 – 0.028 $M_{\odot}$ (Pan et al. 2012; Liu et al. 2013b) of helium-rich material may instead pollute the innermost ejecta of the SN Ia. Liu et al. (2013b) suggest looking for helium lines in this situation, but as discussed in Lundqvist et al. (2013), owing to this pollution, helium lines are not expected to be as prominent as lines of oxygen and calcium. In addition to looking for hydrogen via Hα, we also search here for oxygen and calcium lines with a width of $\sim$1000 km s^{-1}.

In our analysis, we use the same computer code to calculate the line emission from ablated mass from the SD companion as in our previous similar analyses (Mattila et al. 2005; Lundqvist et al. 2013). This is the model discussed in Lundqvist et al. (2013), which is based on calculations for the W7 model (Nomoto et al. 1984; Thielemann et al. 1986). Details of the modelling of late SN Ia spectra using this code for W7 are described in Sollerman et al. (2004) and in Kozma et al. (2005) for other explosion models. The results in Mattila et al. (2005) for the modelled Hα luminosity were extrapolated by Leonard (2007) and Shappee et al. (2013) to obtain the limits on ablated mass in those studies.

While SN 2014J is much closer to us than SN 2011fe, SN 2014J is more extinguished. One could therefore expect SN 2014J to be about as sensitive in terms of the limits on polluting mass from a SD donor, as was reported for SN 2011fe (Shappee et al. 2013). For a comparison between the two supernovae, we include them both in our analysis. Throughout the paper we adopt the distances 6.1 Mpc and 3.4 Mpc to SNe 2011fe and 2014J, respectively. For the Galactic extinction (R_V = 3.1), we use $E(B-V)$ = 0.026 mag for SN 2011fe and $E(B-V)$ = 0.06 mag for SN 2014J. For SN 2014J we also add $E(B-V)$ = 1.37 mag (R_V = 1.4) for M82. We refer to Amanullah et al. (2014), Foley et al. (2014), Goobar et al. (2014), and Johansson et al. (2014) for a discussion of those values. For the recession velocities to the supernovae, we use the host galaxy recessions, i.e., +241 ± 2 km s^{-1} for SN 2011fe and +203 ± 4 km s^{-1} for SN 2014J (de Vaucouleurs et al. 1991). In Sect. 2 we describe our observations and the data, in Sect. 3 we show our results, and in Sect. 4 we provide a discussion. Finally, in Sect. 5 we make our conclusions.

2. Observations

2.1. Observations of SN 2011fe

SN 2011fe was observed on 2012 Jun. 12.16 (JD 2456090.66), i.e., 294 days after the explosion on 2011 Aug. 23.7 for two full hours with the MODS spectrograph on the 8.4-m LBT[1]. The spectrum was first published by Shappee et al. (2013) and then again by McClelland et al. (2013). We have absolute-calibrated the spectrum by comparison to the R-band photometry by Munari et al. (2013). The spectrum is shown in Fig. 1.

2.2. Observations of SN 2014J

We observed SN 2014J with the Nordic Optical Telescope (NOT) on 2014 Nov. 26, i.e., 315 days after the explosion on Jan. 14.75 (Zheng et al. 2014). The NOT observations were made in service mode under NOT proposal 50-023 (P.I. A. Nyholm). The ALFOSC spectrograph was used with grism #8 and a 1.″0 slit (parallactic slit orientation) to get four longslit spectra with exposure time of 1800 s per spectrum. The setup allowed us to obtain spectral coverage of the interval 5820–8370 Å, where the features of interest in this investigation can be found. The expected resolution for our setup with a 1.″0 slit is $\Delta\lambda$ = 7.0 Å. The resolution of the obtained spectra was estimated using night sky lines on each side of Hα in the individual spectra and was found to be between 7.1 Å and 7.8 Å. At the time of the observations, there were thin clouds and variable seeing (extremes: 0.″9 and 1.″3). The UT date for the mid-exposure times of the first and last frames were 2014 Nov. 26.11 and 2014 Nov. 26.17. The spectra were obtained in the airmass range 1.43–1.74 and were reduced in the standard way with IRAF[2] applying overscan corrections, bias subtractions, and flat fields to the individual spectra. The flat fields used were taken with the telescope pointing at the SN, directly before the SN spectra themselves were taken. A He–Ne lamp was used for the wavelength calibration, and Feige 34 was used as flux standard for the four extracted, sky-subtracted SN spectra. The four individual SN spectra were then co-added. The R-band (Bessel) magnitude 17.599 ± 0.041 of SN 2014J had been measured with the NOT on 2014 Nov. 25, and this photometry was used for the absolute flux calibration of the final co-added spectrum. The co-added and flux-calibrated spectrum is shown in Fig. 1.

[1] The Large Binocular Telescope (LBT) and Multi-Object Dual Spectrograph (MODS; Pogge et al. 2013).

[2] IRAF is distributed by the National Optical Astronomy Observatories, which are operated by the Association of Universities for Research in Astronomy, Inc., under cooperative agreement with the National Science Foundation.

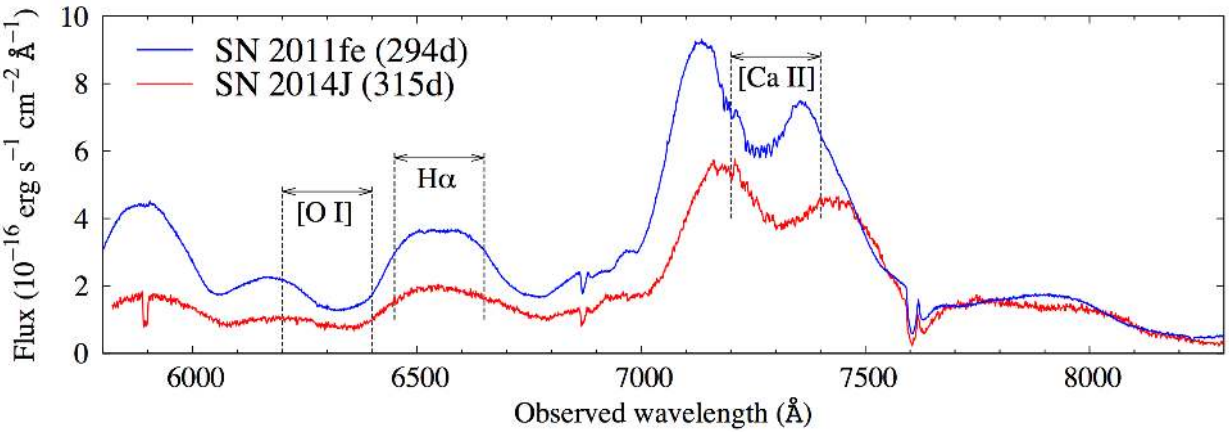

Fig. 1. Observed LBT spectrum (blue colour) of SN 2011fe at 294 days after the explosion (cf. Shappee et al. 2013, for the full LBT spectrum of the supernova) and the observed NOT spectrum (red colour) of SN 2014J 315 days after the explosion. No reddening or redshift correction has been made to the spectra. The recession velocities of the SNe are similar at only 241 km s^{-1} and 203 km s^{-1}, respectively. The wavelength regions of interest for this study are marked with dashed lines and arrows. Those wavelength regions are the same as in Figs. 2 and 3. We note the general blueshift of the broad double-peak between 7000–7500 Å for SN 2011fe relative to SN 2014J, whereas for the peak between 6400–6750 Å, there is no obvious shift in wavelength. See text for further details.

3. Results

In Sects. 3.1 and 3.2, we discuss a strict statistical approach to estimating the upper limits on the tentative line emission from the ablated gas. In Sect. 3.3 we evaluate to what extent these statistical limits can be used to really set lower limits or whether systematic effects dominate.

3.1. SN 2011fe

With the LBT spectrum we initiated our statistical approach in a similar way to what was done in Shappee et al. (2013); i.e., we smoothed the spectrum using a second-order Savitzky-Golay polynomial (Press et al. 1992). We then subtracted the non-smoothed spectrum from the smoothed one, creating a net spectrum. Like Shappee et al. (2013), we found that a smoothing width of ±30 Å produced optimal net spectra.

Net spectra are shown in the left panels of Fig. 2 for the spectral regions around Hα, [O I] λ6300 and [Ca II] $\lambda\lambda$7291, 7324, i.e., lines that are expected from ablated gas of a SD companion (Lundqvist et al. 2013). For our further analysis, we binned the net spectra in 10 Å bins, which is shown in the same way in these figure panels. The 10 Å binning was chosen to obtain enough spectral bins per expected line and to get enough spectral bins to study the noise within a reasonable wavelength region (see below). At the same time, 10 Å binning is fine enough to detect narrow absorption and emission features that do not arise in the SN.

To investigate the noise distribution of the binned net spectra in the wavelength regions of Hα, [O I] λ6300 and [Ca II] $\lambda\lambda$ 7291, 7324, we sampled fluxes in 40 wavelength bins around the wavelength of the modelled spectral lines and compared that to the normal distribution, using a quantile-quantile test (Rice 2007). Prior to estimating the standard deviations, we removed the spectral bins including the features at ~6275 Å and ~6520 Å, marked as telluric features by Shappee et al. (2013). In a quantile-quantile plot, a deviation from a straight line reveals a non-Gaussian distribution. As can be seen in the right-hand panels of Fig. 2, the noise does not deviate appreciably from that of a normal distribution, except for the [Ca II] lines.

The estimated standard deviation and its estimated 95% confidence level (Rice 2007) for the 6350–6750 Å, 6100–6500 Å and 7100–7500 Å spectral regions are $(6.90^{+2.10}_{-1.19}) \times 10^{-19}$ erg s^{-1} cm^{-2} Å^{-1}, $(4.43^{+1.35}_{-0.76}) \times 10^{-19}$ erg s^{-1} cm^{-2} Å^{-1}, and $(4.70^{+1.41}_{-0.80}) \times 10^{-18}$ erg s^{-1} cm^{-2} Å^{-1} for each spectral region, respectively. For each spectral region, we used the maximum standard deviation within its 95% confidence level range to make a robust estimate of the 1σ noise of the spectral bins of the expected line profiles.

Model spectra were obtained from interpolation in time, and inter- and extrapolation in ablated mass using the grid of models in Lundqvist et al. (2013) where the masses were varied between 0.01–0.50 $M_\odot$. Extrapolation to lower masses than 0.01 $M_\odot$ works well for all lines considered here because collisional de-excitation of even [O I] λ6300 is unimportant for such low masses. We applied appropriate redshift and reddening to the model spectra, mapped them onto the 10 Å spectral grid, and created 10 000 artificial spectra by adding noise using the Monte Carlo method, where the noise was estimated from the maximum standard deviations at a 95% confidence level. We ranked the simulated line fluxes, and for each line (or doublet in case of [Ca II]), we estimated 1σ errors from those ranked in places 1587 and 8413. A 3σ statistical upper limit to the ablated mass was estimated from the mass that gives a 1σ limit of the flux that is three times lower than the modelled line flux. The left-hand panels of Fig. 2 show the modelled line profiles (in blue) for those masses, as well as those when mapped onto the spectral grid. For [O I], we excluded the weak [O I] λ6364 component from the analysis, because this does not add any important constraints on the oxygen mass.

For Hα we estimated that solar-metallicity ablated material with a mass of 0.0010 $M_\odot$ would have been enough to detect in the LBT spectrum. This is fully consistent with the upper limit of 0.001 $M_\odot$ reported by Shappee et al. (2013). For [O I] λ6300 and [Ca II] $\lambda\lambda$7291,7324, we estimated that at least 0.0023 $M_\odot$ and 0.0086 $M_\odot$, respectively, of ablated material with solar metallicity are needed to result in a detection. These masses correspond to the observed line fluxes of 7.0×10^{-17} erg s^{-1} cm^{-2}, 4.6×10^{-17} erg s^{-1} cm^{-2}, and 5.5×10^{-16} erg s^{-1} cm^{-2}. The relatively high limit from the [Ca II] lines is due to a noisy region in the spectrum between ~7150–7350 Å (cf. Fig. 1) hampered by the atmosphere.

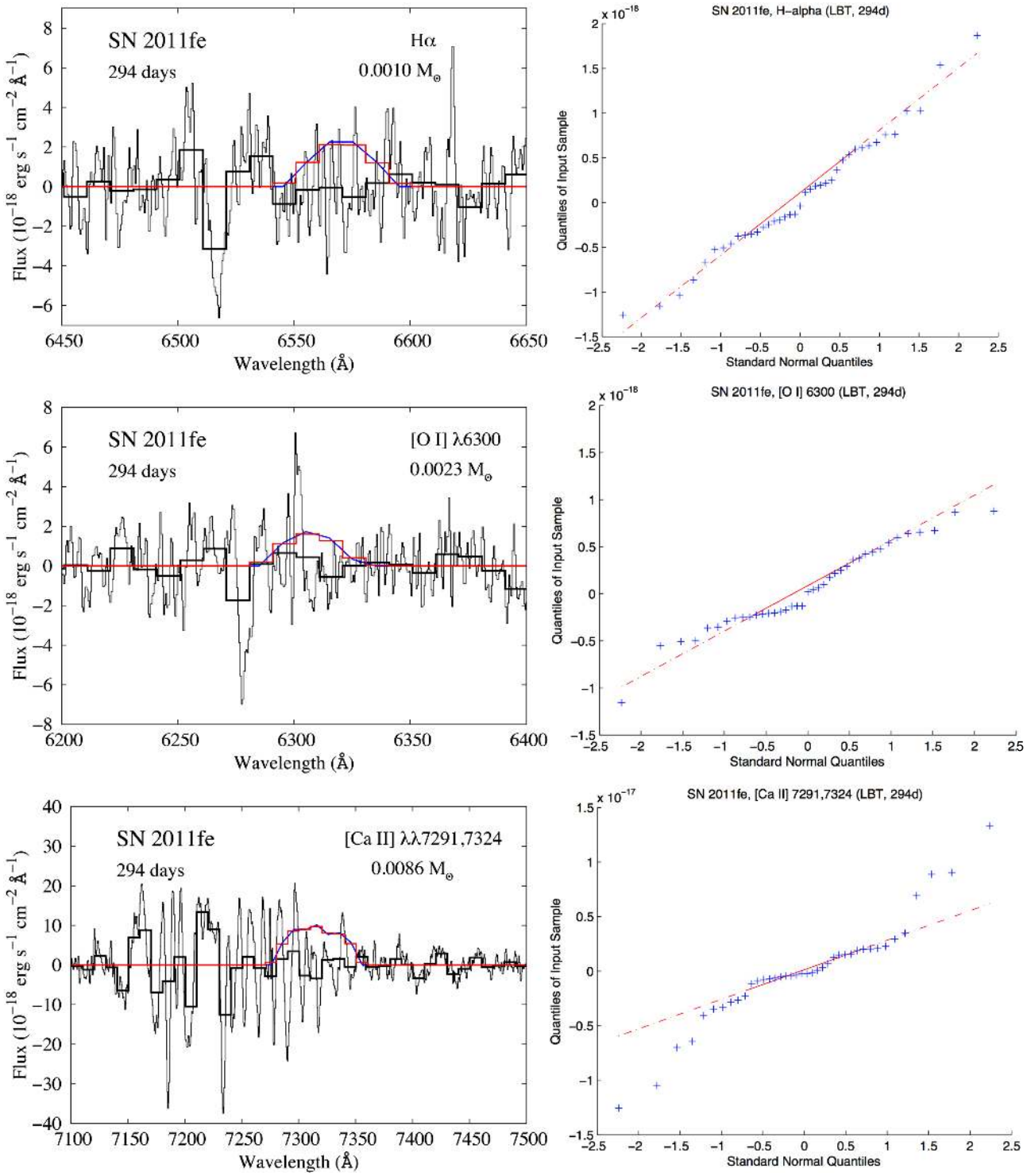

Fig. 2. *Left columns*: LBT net spectra (i.e., spectra after continuum removal) of SN 2011fe 294 days after the explosion (thin black lines) in the spectral regions around Hα (*upper panel*), [O I] λ6300 (*middle panel*), and [Ca II] $\lambda\lambda$7291, 7324 (*lower panel*), respectively. The thick black histogram lines show the observed spectrum after 10 Å binning. No correction for redshift was made. The blue lines show the modelled line emission, using the model in Lundqvist et al. (2013) for 294 days. The red histogram lines show the modelled flux binned to the same resolution as the binned observed spectrum. The mass of solar-metallicity material in these models are 0.0010 $M_{\odot}$, 0.0023 $M_{\odot}$, and 0.0086 $M_{\odot}$, respectively, and correspond to estimated 3σ statistical upper limits of the mass. The modelled spectra have been redshifted by +203 km s^{-1} and reddened by $E(B-V) = 0.026$ mag to match the velocity and extinction of the supernova. A distance of 6.1 Mpc was used. The mass limit for Hα agrees with that of Shappee et al. (2013) using the same data. *Right columns*: quantile-quantile plots of the data in the net spectra. Blue data points are from the distribution of binned fluxes (in 10 Å bins) for 400 Å spectral regions around the modelled lines. The dashed red lines are for the simulated normal distribution. As can be seen, the data samples do not deviate appreciably from a normal distribution, except for the [Ca II] lines. The spectral bins dominated by telluric features at ~6275 Å and ~6520 Å (cf. Shappee et al. 2013) were removed from the sample prior to analysis. See text for further details.

3.2. SN 2014J

The NOT spectrum of SN 2014J was also smoothed using a second-order Savitzky-Golay polynomial, and a net spectrum was created from this as was done for SN 2011fe in Sect. 3.1. Again, we smoothed the spectrum with a width of ±30 Å. The net spectra for the spectral regions around Hα, [O I] λ6300 and [Ca II] $\lambda\lambda$7291,7324 are shown in the left-hand panels of Fig. 3. For further analysis, we binned the net spectra in 10 Å bins, as shown in these panels of Fig. 3.

The noise distribution of the binned net spectra in the wavelength regions of Hα, [O I] λ6300 and [Ca II] $\lambda\lambda$7291, 7324 was investigated in the same way as for SN 2011fe in Sect. 3.1. The quantile-quantile plots for the noise distribution around those lines are shown in the right-hand panels of Fig. 3. Unlike for SN 2011fe, we did not remove any outliers prior to the noise estimate. As can be seen in the right-hand panels of Fig. 3, the noise is represented well by that of a normal distribution. There is only one obvious outlier, the emission feature around 7210 Å in the lower left-hand panel of Fig. 3 (cf. Sect. 4.3).

The estimated standard deviation, and its estimated 95% confidence level, for the 6350–6750 Å, 6100–6500 Å and 7100–7500 Å spectral regions are $(1.78^{+0.53}_{-0.30})\times10^{-18}$ erg s^{-1} cm^{-2} Å^{-1}, $(1.51^{+0.45}_{-0.26})\times10^{-18}$ erg s^{-1} cm^{-2} Å^{-1}, and $(6.06^{+1.82}_{-1.03})\times10^{-18}$ erg s^{-1} cm^{-2} Å^{-1} for each spectral region, respectively. As for SN 2011fe in Sect. 3.1, we used the maximum standard deviation within its 95% confidence level range to estimate the 1σ statistical uncertainty for the spectral bins of the expected line profiles. Comparing the standard deviation uncertainties for SN 2014J with the 1σ uncertainties for SN 2011fe, it can be noted that the NOT spectra are somewhat noisier than the LBT spectra in the spectral regions of Hα and [O I] λ6300, whereas the noise levels are about the same for the [Ca II] $\lambda\lambda$7291,7324 spectral region. This agrees with a visual inspection of the left-hand panels of Figs. 2 and 3.

For Hα and [O I] λ6300, we estimated that solar-metallicity ablated material with a mass of 0.0035 $M_\odot$ and 0.0096 $M_\odot$, respectively, would have been enough to detect these lines in the NOT net spectrum. These are factors of 3–5 higher than for SN 2011fe, mainly owing to the higher extinction towards SN 2014J and the smaller telescope size of the NOT compared to the LBT. For [Ca II] $\lambda\lambda$7291, 7324, we estimate that at least 0.006 $M_\odot$ of ablated material with solar-metallicity is needed to result in a detection. This is below the limit for SN 2011fe because of the modest extinction for SN 2014J in the red, as well as in a noisy region of the LBT spectrum at wavelengths that partly overlap those expected for the [Ca II] lines.The upper mass limit on ablated masses from Hα, [O I] λ6300 and [Ca II] $\lambda\lambda$7291,7324 correspond to observed line fluxes of 1.6×10^{-16} erg s^{-1} cm^{-2}, 1.3×10^{-16} erg s^{-1} cm^{-2} and 3.8×10^{-16} erg s^{-1} cm^{-2}, respectively.

3.3. Sanity check of results

The estimated 3σ limits on ablated mass in Sects. 3.1 and 3.2 are strictly statistical. Additional systematic errors may arise owing to our ignorance of the shape of the underlying spectrum from the supernova ejecta. The statistical approach artificially removes this uncertainty when the smoothed continuum is subtracted from the observed one. To highlight this, Fig. 4 shows the observed spectra and compares that to smoothed spectra plus modelled line emission.

3.3.1. Hα

The upper panel of Fig. 4 shows the region around Hα for both supernovae. For SN 2014J we indicate a subtraction of a spectrum corresponding to the 3σ statistical limit. An inspection by eye shows that the 3σ statistical limit could easily be taken as part of the supernova continuum for SN 2011fe. For a clear deviation from the general shape of the continuum, one should probably require three times the 3σ statistical limit for SN 2011fe and somewhat less than $3\times3\sigma$ for SN 2014J to also include systematic uncertainties. This means that the limit on ablated mass from Hα should be ~0.003 $M_\odot$ for SN 2011fe and ~0.0085 $M_\odot$ for SN 2014J.

3.3.2. [O I] λ6300

The middle panel of Fig. 4 shows the region around [O I] λ6300. The blue, red, and black lines have the same meaning as for the Hα panel. An inspection by eye shows that 3× the 3σ statistical limit is probably a safe upper limit for SN 2011fe, whereas 2× the 3σ statistical limit should certainly be enough for SN 2014J. This translates into upper limits on ablated mass using [O I] λ6300 of ~0.007 $M_\odot$ for SN 2011fe and ~0.02 $M_\odot$ for SN 2014J.

3.3.3. [Ca II] $\lambda\lambda$7291, 7324

The lower panel of Fig. 4 shows the region around [Ca II] $\lambda\lambda$7291, 7324 for both supernovae. For SN 2011fe even more than 5× the 3σ statistical limit produces a spectrum that could mistakenly be part of the supernova continuum bump around ~7350 Å, whereas five times the 3σ statistical limit is probably a fair upper limit to the ablated mass for SN 2014J. This corresponds to a limit on ablated mass from [Ca II] $\lambda\lambda$7291, 7324 which is ~0.06 $M_\odot$ for SN 2011fe and ~0.03 $M_\odot$ for SN 2014J.

4. Discussion

The limits on ablated mass in Sect. 3 were derived under the assumption of solar abundance composition (Anders & Grevesse 1989). This is expected in a SD scenario where hydrogen-rich gas is stripped from the companion star. However, there is also the possibility that helium-dominated gas is stripped (Pan et al. 2012; Liu et al. 2013b). If the O/He and Ca/He ratios and the efficiency of line emission in such a scenario do not deviate significantly from the solar composition case, our results may provide rough upper limits to the ablated mass in case of a helium-rich donor. The upper limits from [O I] λ6300 and [Ca II] $\lambda\lambda$7291, 7324 will then be a factor of $4([X_{\rm He}/X_{\rm H}]/(1+4(X_{\rm He}/X_{\rm H})))$ lower than in Sect. 3. Here $X_{\rm He}/X_{\rm H}$ is the number density ratio of He and H for solar abundance. With $X_{\rm He}/X_{\rm H}=0.085$, this factor becomes ≈0.25, meaning that the upper limits on ablated mass from Sects. 3.2.2. and 3.2.3. become ~0.002 $M_\odot$ and ~0.005 $M_\odot$ using [O I] λ6300 and ~0.015 $M_\odot$ and ~0.008 $M_\odot$ using [Ca II] $\lambda\lambda$7291, 7324 for SNe 2011fe and 2014J, respectively.

In Fig. 5 we summarise the predicted ablated masses and the upper limits from observations. We include both hydrogen- and helium-rich donors, where the predicted ablated masses for hydrogen-rich donors were taken from Pan et al. (2012) and those expected in the helium-rich case from Pan et al. (2012) and Liu et al. (2013b). For the results of Pan et al. (2012), we used the information in their Table 2, while for the results of

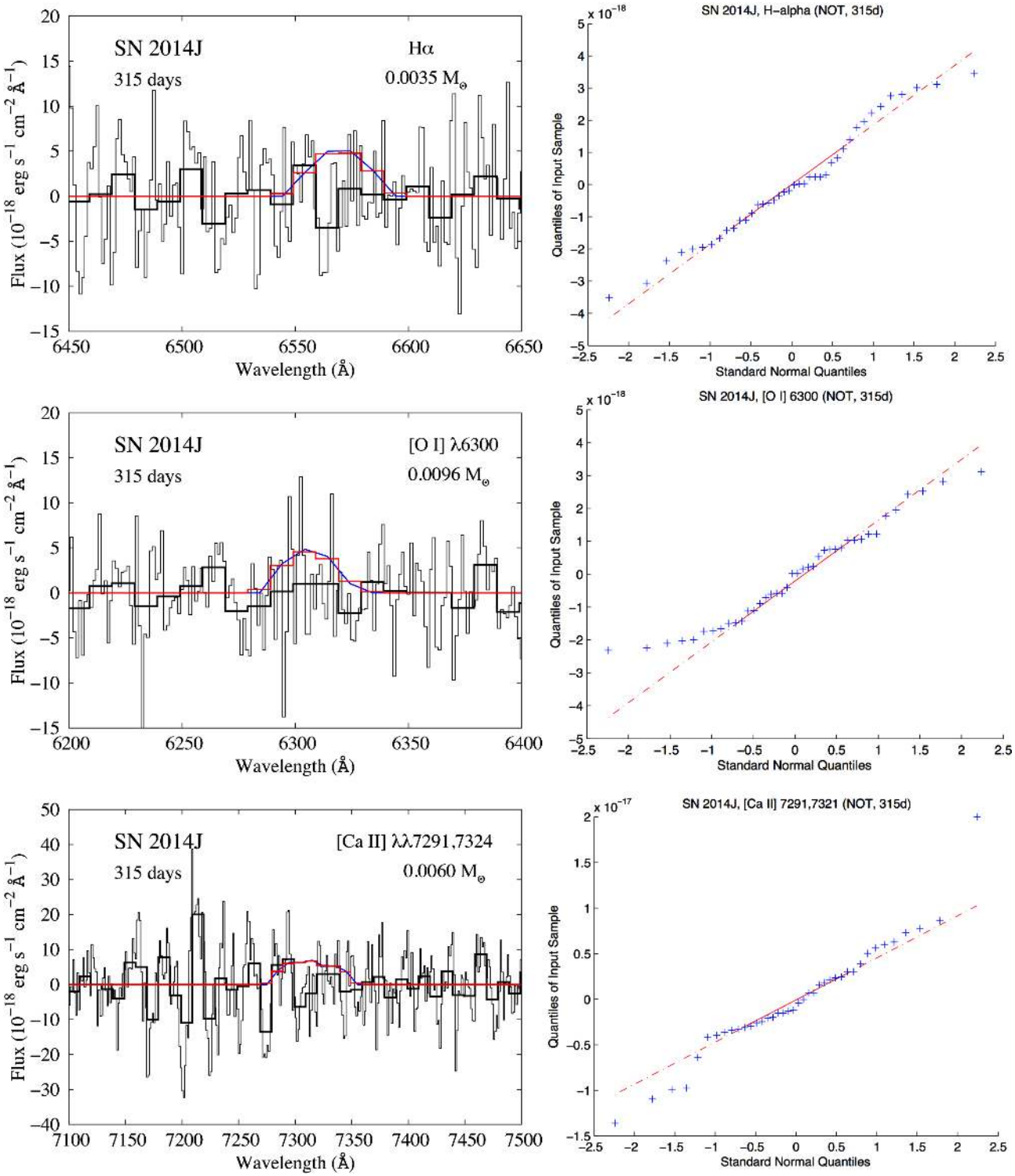

Fig. 3. *Left columns*: NOT net spectra (i.e., spectra after continuum removal) of SN 2014J around Hα (*upper panel*), [O I] λ6300 (*middle panel*), and [Ca II] $\lambda\lambda$7291, 7324 (*lower panel*). The thick black histogram lines show the observed spectrum after 10 Å binning. No correction for redshift was made. The blue lines show the modelled line emission, using the model in Lundqvist et al. (2013) for 315 days. The red histogram lines show the modelled flux binned to the same resolution as the binned observed spectrum. The mass of solar-metallicity material in these models are 0.0035 $M_{\odot}$, 0.0096 $M_{\odot}$, and 0.0060 $M_{\odot}$, respectively, and they correspond to the estimated 3σ statistical upper limits of the mass. The modelled spectrum has been redshifted by +241 km s^{-1} and reddened according to what is given in Section 1 to match the redshift and extinction of the supernova. A distance of 3.4 Mpc was used. *Right columns*: quantile-quantile plots of the data in the net spectra. Blue data points are from the distribution of binned fluxes (in 10 Å bins) for 400 Å spectral regions around the modelled lines. The dashed red lines are for the simulated normal distribution. As can be seen, the data samples do not deviate appreciably from a normal distribution, except for the strongest absorption features around the [O I] line, and the strongest emission feature in the [Ca II] spectrum in the lower left panel. No spectral bins were, however, removed from the sample prior to analysis. See text for further details.

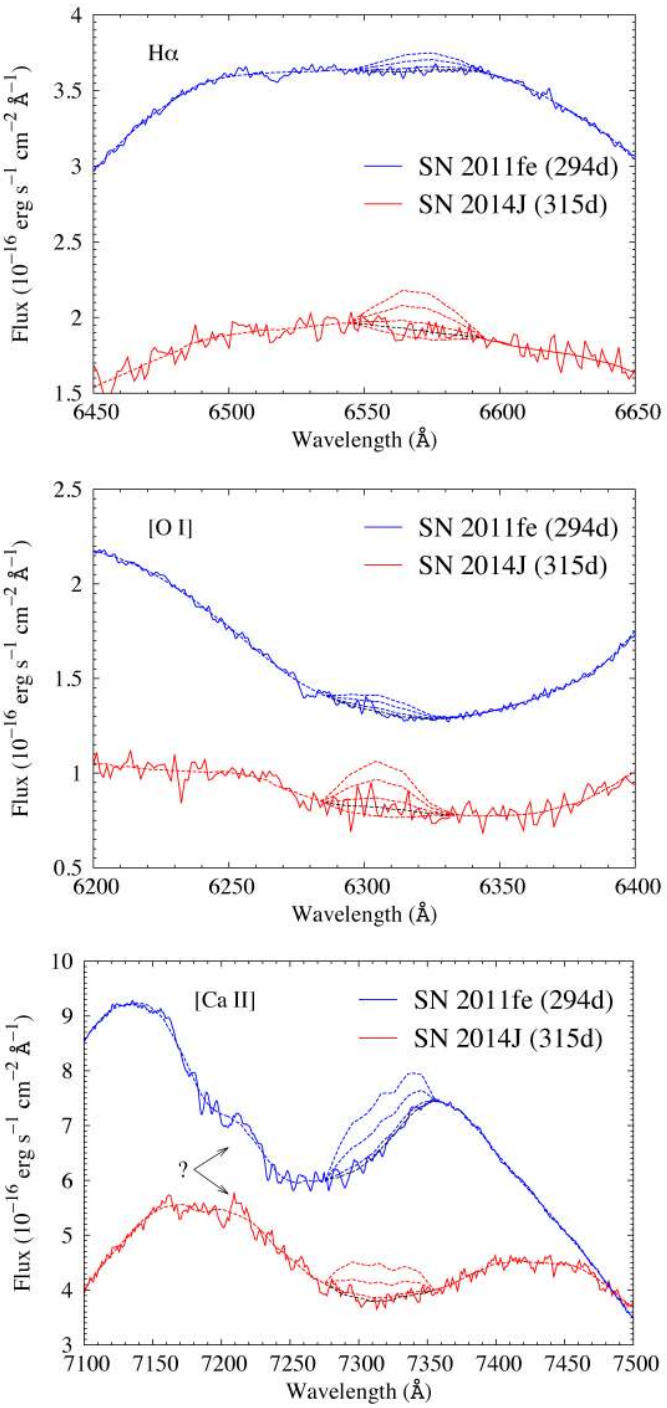

Fig. 4. Observed spectra (solid red and blue lines) with modelled line profiles (dashed red and blue lines) added. For Hα (*upper panel*) and [O I] λ6300 (*middle panel*), the modelled fluxes are for 1×, 3×, and 5× the 3σ statistical limits on the masses estimated in Sects. 3.1 and 3.2. For Hα and [O I] λ6300 we also subtracted 1× these masses (also shown by red dashed lines). For [Ca II] $\lambda\lambda$7291,7324 (*lower panel*), we added modelled fluxes corresponding to 1×, 5×, and 10× the 3σ statistical limits on the masses estimated in Sects. 3.1 and 3.2. The dashed lines (marked in black across the line profiles) tracing the full observed spectra are the smoothed spectra using Savitzky-Golay polynomials, as outlined in Sects. 3.1 and 3.2. In the [Ca II] $\lambda\lambda$7291,7324 panel, we have highlighted a feature around 7210 Å present in the spectra of both supernovae with a question mark. The plots show observed wavelengths.

Liu et al. (2012, 2013b) we followed the advice in Liu et al. (2013b) to assume that 50% of the gas lost from the companion because the supernova impact is ablated. The mass range of ablated hydrogen-rich gas is therefore 0.052–0.091 $M_\odot$ according to Liu et al. (2012, which supersedes the models of Pakmor et al. 2008) or 0.0139–0.636 $M_\odot$ according to Pan et al. (2012), while for the helium-rich case in Fig. 5, we indicate the ranges 0.00245–0.0134 $M_\odot$ (Pan et al. 2012) and 0.0095–0.028 $M_\odot$ (Liu et al. 2013b).

Our limits are sensitive to the velocity of the stripped or ablated gas. We assumed that the ablated gas is confined to 10^3 km s^{-1}. This assumption agrees with the results of Pan et al. (2012), where the peak of the velocity distribution is well below 10^3 km s^{-1} for hydrogen-rich donors, but just short of this velocity for helium-rich donors (see also Liu et al. 2013b, for a confirmation); there is a significant fraction of gas with velocities in the range (1–2) × 10^3 km s^{-1} in the helium-donor case. A higher velocity than our assumed 10^3 km s^{-1} results in shallower emission line profiles from the ablated gas, and the limits on ablated gas for helium-rich donors should therefore be shifted upwards in Fig. 5. Judging from the velocity distribution of the ablated gas in Pan et al. (2012), the upward shift could be a factor of ∼1.3–1.5, whereas for hydrogen-rich donors, the factor could instead be shifted in the other direction by a similar amount since the expected velocity of the ablated gas is well below 10^3 km s^{-1} for such donors.

4.1. Implications for SNe 2011fe and 2014J

4.1.1. Constraints from our findings

From Fig. 5 it is obvious that hydrogen-rich donor stars are disfavoured for both SNe 2011fe and 2014J. Pan et al. (2012) made models for both red-giant and main-sequence companions, and the main-sequence stars populate the lower part of the range marked "Liu12" in Fig. 5. Red-giant hydrogen-rich companions for SNe 2011fe and 2014J are therefore clearly ruled out in terms of ablated mass. The models with the lowest amount of ablated gas are those with main-sequence companions, and among these the ablated mass decreases with increasing orbital separation. The largest separation tested by Pan et al. (2012) was 2.75×10^{11} cm, corresponding to 5 $R_\star$, where $R_\star$ is the donor star radius. They found a power-law relation between the separation (in units of $R_\star$) and the amount of unbound matter from the donor. Extrapolating their grid of models, the separation would need to be $\gtrsim$6 $R_\star$ for the ablated mass to be as low as our upper limit for SN 2014J, and $\gtrsim$8.5 $R_\star$ for SN 2011fe. Models with these large separations were tested by Pakmor et al. (2008),who found that the stripped mass could be below 0.01 $M_\odot$ for models with a large separation, and even lower if the explosion energy is reduced. Although the trends are clear, the exact numbers in Pakmor et al. (2008) are uncertain, as warned about in Liu et al. (2012) and Pan et al. (2012).

While the models explored by Pan et al. (2012) used the binary evolution models of Ivanova & Taam (2004) as input, Liu et al. (2012) modelled both the binary evolution and simulated the explosion impact themselves. Liu et al. (2012) concentrated on main-sequence companions, and like Pan et al. (2012), they found a clear trend towards decreasing ablated mass for increasing binary separation when expressed in $R_\star$. The ablated mass is, however, higher than in the models of Pan et al. (2012), and our mass limits on ablated hydrogen-rich gas for both SNe 2011fe and 2014J are much lower than in the models of Liu et al. (2012). It remains to be tested which of the impact simulations are the most accurate in terms of ablated mass. In any case, a large separation is needed to make the impact models compatible with our limits on ablated hydrogen-rich gas.

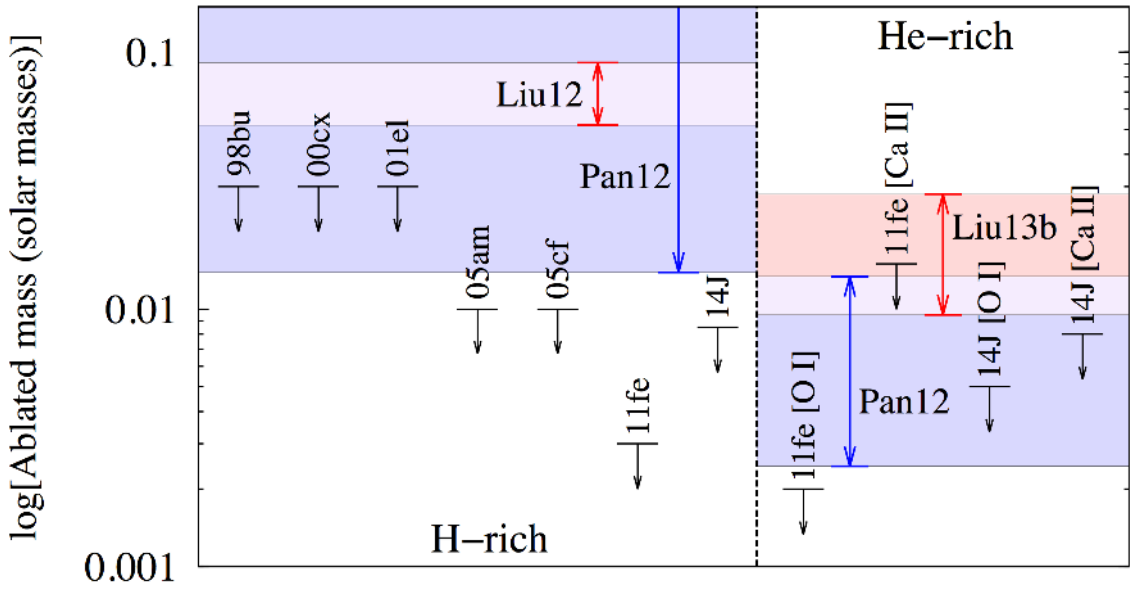

Fig. 5. Summary of estimated upper limits on the mass of ablated gas from a SD companion. The estimates for SNe 1998bu and 2000cx are from Lundqvist et al. (2013), the one for SN 2001el from Mattila et al. (2005), the ones for SNe 2005am and 2005cf from Leonard (2007), and the ones for SNe 2011fe and 2014J are from this paper. The left part of the figure is for hydrogen-rich gas, and the right part for helium-dominated gas. Simulated ranges of ablated mass are marked by filled areas and arrows. For hydrogen-rich donors, red is for Liu et al. (2012) and blue for Pan et al. (2012), while for helium-dominated donors, red is for Liu et al. (2013b) and blue for Pan et al. (2012). Our limits for both SNe 2011fe and 2014J are below the simulated ranges for hydrogen-rich gas, while helium-rich donors cannot be fully ruled out, in particular not for SN 2014J, if we are guided by the simulations of Pan et al. (2012). See text for further details.

If the SD companion were instead a helium-rich donor, the right-hand part of Fig. 5 shows that it is only our limits for SN 2011fe that are below the expected mass of ablated gas from impact models. However, if one adjusts for a likely slightly higher velocity of the ablated gas for helium-rich donors than assumed in the construction of Fig. 5, we cannot rule out all models of helium-rich donors in Pan et al. (2012), even for SN 2011fe. For SN 2014J, our upper limits from both [O I] λ6300 and [Ca II] $\lambda\lambda$7291,7324 are higher than the lower part of the range of ablated masses in the models of Pan et al. (2012). As for the hydrogen-rich case, it is the systems with the largest separation that produce the least amount of helium-rich ablated gas in these models. The helium-rich companion in Pan et al. (2012) is from Wang et al. (2009), and not from simulations of binary evolution. There could therefore be some uncertainty regarding the binary evolution, and thus perhaps the amount of ablated gas. Liu et al. (2012), on the other hand, follow the detailed binary evolution leading up to the explosion. The smallest amount of unbound material from the companion occurs for the systems with the largest separation. As for hydrogen-rich companions, there is an inconsistency between the impact models of Liu and co-workers and Pan et al. (2012) with regard to the amount of ablated mass. Until this is settled, it must be admitted that the progenitor system of SN 2014J, and perhaps even that of SN 2011fe, could have been a WD with a helium-rich non-degenerate companion at a large separation.

4.1.2. Checking against other constraints on SNe 2011fe and 2014J

Pre-explosion imaging of SN 2011fe (Li et al. 2011) cannot fully rule out a helium-rich donor as the origin of the system. Donors with $M_V \gtrsim -0.6$ mag, in combination with $T_{\rm eff} \gtrsim 50\,000$ K, are allowed. Here M_V is the absolute visual magnitude of the donor at the time of explosion. Using the bolometric corrections of Torres (2010), the bolometric luminosity of a tentative helium-rich donor in the SN 2011fe progenitor system was $\log(L_{\rm bol}/L_{\odot,\rm bol}) \lesssim 3.5$. Most of the helium-donor stars in Liu et al. (2013b) and Wang et al. (2009, who thoroughly investigated helium-donor systems) have properties in this range, so our analysis (cf. Fig. 5) could be more constraining than the pre-explosion imaging, especially if the impact models of Liu et al. (2013b) are closer to the real situation than those of Pan et al. (2012) in terms of ablated gas.

Related to our results for SN 2011fe is the *Swift* study by Brown et al. (2012). The non-detection of very early ultraviolet emission from the supernova limits the parameter space of allowed SD companions to only include main-sequence companions with masses $\lesssim$2–3.5 $M_\odot$, and perhaps even $\lesssim$1 $M_\odot$ for close companions. Geometric probabilities are less than 1% for a 2 (1) $M_\odot$ main-sequence star separated from the white dwarf by 5(3) $\times$ 10^{11} cm – i.e., close to the largest separation of 3×10^{11} cm tested by Pan et al. (2012) for hydrogen-rich companions – and decreases further for larger separation. Our analysis for SN 2011fe, in combination with the models of Pan et al. (2012), rules out a SD system with a hydrogen-rich donor at a separation of $\lesssim$8.5 $R_\star \sim 4 \times 10^{11}$ cm. Adding the constraints from the analysis of the *Swift* observations essentially rules out all SD scenarios with a main-sequence hydrogen-rich donor for SN 2011fe. A 2–3 $M_\odot$ main-sequence star could be possible if it lies within a few degrees along the line of sight on the rear side of the white dwarf. Such a star would also pass the limits set by the pre-explosion imaging (Li et al. 2011), but is likely at odds with the very early optical observations discussed by Bloom et al. (2012).

The only hydrogen-rich SD scenario reasonably possible for SN 2011fe is that of a spun-up/spun-down super-Chandrasekhar WD (Di Stefano et al. 2011; Justham 2011; Hachisu et al. 2012). In such systems the donor star shrinks far inside its Roche lobe prior to the explosion, making the SD companion smaller and

more tightly bound. The supernova ejecta impact on such a star should also produce low enough emission to pass the limits from the early UV observations of Brown et al. (2012). Furthermore, very small amounts of ablated gas are expected, as are very dilute ($n \sim 1\,\mathrm{cm}^{-3}$) circumstellar gas in the vicinity of the supernova. A way to constrain this scenario is through continued deep monitoring of the supernova in radio (Pérez-Torres et al. 2014).

Our results for SN 2011fe are also consistent with previous findings (cf. Maoz et al. 2014) that it may indeed have been the outcome of a DD scenario. What speaks in favour of a DD scenario rather than the spun-up/spun-down super-Chandrasekhar WD scenario is that SN 2011fe was a normal SN Ia in terms of lightcurve and spectral evolution and that the spun-up/spun-down super-Chandrasekhar WD scenario is not thought to be the normal path leading to a SN Ia explosion. However, while the DD scenario for SN 2011fe may be likely, we cannot rule out a spun-up/spun-down super-Chandrasekhar WD. Neither can we fully rule out a helium-rich donor at large separation (cf. above). Using the numbers in Figs. 5 and. 12 in Pan et al. (2012), we estimate that we cannot rule out separations that are $\gtrsim 6\,R_\star \sim 8 \times 10^{10}$ cm and $\gtrsim 4.5\,R_\star \sim 6 \times 10^{10}$ cm for helium-rich donors for SNe 2011fe and 2014J, respectively. Even if not explicitly discussed by Brown et al. (2012), helium-rich donor systems with such small separation may not be well constrained by the early *Swift* observations of SN 2011fe.

Recently, Taubenberger et al. (2015) have reported very late (1034 days past explosion) observations of SN 2011fe. No sign of narrow Hα was found, but this could be due to a poor signal-to-noise ratio. A tentative identification of [O I] was, however, made, which would make SN 2011fe the third SN Ia ever, besides SNe 1937C (Minkowski 1939) and the subluminous 2010lp (Taubenberger et al. 2013), to show signs of [O I] in late spectra. The [O I] emission in SN 2010lp is unlike what we expect from ablated gas since the line profiles indicate emission at velocities offset by $\sim$1900 km s^{-1} from the rest wavelengths of [O I] $\lambda\lambda$6300, 6364. If the [O I] identification is correct for SN 2011fe, then a similarly large offset ($\sim$+2000 km s^{-1}) would apply. The [O I] emission in these SNe has therefore probably nothing to do with ablated gas from a companion, but should come from blobs of oxygen-rich SN ejecta. In the case of SN 2011fe, we emphasise that the [O I] identification could also be a misinterpretation, since the emission may very well be due to iron (Taubenberger et al. 2015).

As for SN 2011fe, the progenitor system for SN 2014J, could have been a DD system, a spun-up/spun-down super-Chandrasekhar WD scenario, or a system with a helium-rich companion at large separation. For SN 2014J, our results could also be compatible with a well-separated hydrogen-rich donor system. A recent clue, perhaps in favour of a SD scenario, was the reported early variation in two narrow absorption components of K I λ7665 (Graham et al. 2014). The estimated distance from the supernova to the absorbing gas is, however, $\sim 10^{19}$ cm, which is $\sim$50–100 times further away from the supernova than the likely position of a circumstellar blast wave after one year (Pérez-Torres et al. 2014). Continued monitoring in radio may pick up circumstellar gas closer to the supernova. Unlike narrow absorption lines, radio is sensitive to any gas close to the supernova, and not only gas along the line of sight to it.

Further clues to the origin of SN 2014J come from the very early photometry of the supernova. As reported by Goobar et al. (2015), the rise in luminosity during the first few days after explosion indicates an extra energy source that could be due to interaction of the ejecta with a non-degenerate companion (cf. Kasen 2010) or the debris from a disrupted WD (e.g., Levanon et al. 2015). The matter interacting with the ejecta must be confined to the immediate vicinity of the explosion site since radio observations only eight to nine days after the explosion did not reveal any emission (Chandler & Marvil 2014; see also Pérez-Torres et al. 2014).

Analysis of pre-explosion images (Kelly et al. 2014) shows that a DD progenitor system, a helium-star donor with low effective temperature ($T_{\rm eff}$), or a system like U Sco (recurrent nova and a supersoft-X-ray source with a subgiant companion) would not show up in the pre-explosion images. On the other hand, SD systems, such as V445 Pup (bright helium-star donor) or RS Oph (bright recurrent nova and a symbiotic source), are both excluded.

More specifically, the pre-explosion imaging of SN 2014J cannot rule out helium-star donors with $M_V \gtrsim -2.5$ mag in combination with $T_{\rm eff} \gtrsim 40\,000$ K (cf. Fig. 4 of Kelly et al. 2014). Again, using the bolometric corrections of Torres (2010), the bolometric luminosity of a tentative helium-rich donor in the SN 2014J progenitor system was $\log(L_{\rm bol}/L_{\odot,\rm bol}) \lesssim 4.4$. The helium-donor stars in Liu et al. (2013b) and Wang et al. (2009) all have properties in this range, so our analysis (cf. Fig. 5) is more constraining than the pre-imaging for helium-donor stars, in particular if the simulations of Liu et al. (2013b) are more representative than those of Pan et al. (2012). We note, however, that Liu et al. (2013b) assume that the metal abundance of the helium-rich donor remains at $Z = 0.02$ (i.e., the solar value) even when hydrogen has been removed, whereas we have assumed in Fig. 5 that this number is a factor of 4 higher for helium-rich donors than for hydrogen-rich ones. If we abandon this correction factor, and also consider the slightly higher velocity of the ablated gas in the helium-rich scenario than assumed in Fig. 5, the ablated mass in the models of Liu et al. (2013b) becomes consistent with our results, in particular for the helium-star donors with the largest separation to the WD. Removing the correction factor of 4 could make it easier to accommodate a helium-star donor system also for SN 2011fe. For SN 2014J, we note that a helium-rich donor was argued for by Diehl et al. (2014) to explain the early emergence of gamma-ray line emission.

4.2. Broad lines of SN 2011fe and 2014J

The main spectral peak between 7050–7250 Å for SN 2014J is centred at $\approx$7170 Å, whereas it is shifted to the blue at $\approx$7135 Å for SN 2011fe. This is close to the rest wavelength of [Fe II] λ7155. Likewise, the main peak between 7250–7300 Å and 7500 Å is clearly shifted more to the blue for SN 2011fe, where the peak occurs at $\sim$7355 Å, compared to $\sim$7420 Å for SN 2014J. Most of this peak can be attributed to [Ni II] λ7378. Correcting for the redshifts of the SNe, and assuming that [Fe II] λ7155 and [Ni II] λ7378 are the main contributors (see also Maeda et al. 2010b; Taubenberger et al. 2015; Graham et al. 2015), the [Fe II] λ7155 peak occurs at ~ -1000 km s^{-1} and $\sim$+400 km s^{-1} for SNe 2011fe and 2014J, respectively, whereas for [Ni II] λ7378 they are at ~ -1100 km s^{-1} and $\sim$+1300 km s^{-1} for SNe 2011fe and 2014J, respectively. There is thus a consistent blueshift for SN 2011fe, which is in full agreement with McClelland et al. (2013, see also Graham et al. 2015), whereas the lines are redshifted for SN 2014J. Figure 1 does not show any obvious similar shifts between the supernovae for the broad peaks with centres around 5900 Å and 6550 Å, which are thought to be dominated by [Co III] lines (Maeda et al. 2010b; Taubenberger et al. 2015; Graham et al. 2015). This agrees with

the analysis of Maeda et al. (2010b), where [Fe II] λ7155 and [Ni II] λ7378 mainly originate in the dense central parts of the ejecta where asymmetries can be expected, as opposed to the more highly ionised exterior region, which is closer to being spherically symmetric. Maeda et al. (2010b) argue that this is a natural outcome of a delayed-detonation scenario, and exemplify this for 12 SNe Ia. Half of them have shifts of [Ni II] λ7378 in excess of 1500 km s^{-1}. Both SNe 2011fe and 2014J have smaller velocity offsets, which may be just a viewing angle effect.

According to Maeda et al. (2010a), the viewing angle may also influence how fast the absorption trough of Si II λ6355 recedes after B-band maximum. The decline rate in this velocity ($v_{\rm SiII}$) is called $\dot{v}_{\rm Si}$, and Maeda et al. (2010a) argue that SNe Ia with $\dot{v}_{\rm Si} \gtrsim 70$ km s^{-1} d^{-1} (the so-called high-velocity gradient, or HVG, group, cf. Benetti et al. 2005) all have redshifted [Fe II] λ7155 and [Ni II] λ7378 emission in nebular spectra. There is also a small fraction of those SNe Ia with $\dot{v}_{\rm Si} \lesssim 70$ km s^{-1} d^{-1} (the so-called low-velocity gradient, or LVG, group) that have redshifted nebular lines, but the majority of the LVG group SNe Ia have blueshifted [Fe II] λ7155 and [Ni II] λ7378 emission.

Consulting the results of Kawabata et al. (2014) and Marion et al. (2015) for SN 2014J, we find that $\dot{v}_{\rm Si}$ ~55 km s^{-1} d^{-1} (between 0–30 days after B maximum) and $\dot{v}_{\rm Si}$ ~50 km s^{-1} d^{-1} (between −0.7 and +9.3 days after B maximum), respectively. Furthermore, Ashall et al. (2014) find $\dot{v}_{\rm Si} \approx 58.8$ km s^{-1} d^{-1} between 0–10 days after B maximum using their observations. This would put SN 2014J in the LVG group, and the supernova would belong to the minority of SNe Ia, which are both LVG group objects, and both have redshifted nebular [Fe II] λ7155 and [Ni II] λ7378 emission. Another one in this category is SN 2001el (Maeda et al. 2010a, this SN is discussed further in Sect. 4.4). We note that no LVG SNe in Benetti et al. (2005) have $v_{\rm SiII} \geq 11\,000$ km s^{-1} around B-band maximum, but $v_{\rm SiII} \approx 11\,750$ km s^{-1} for SN 2014J at that epoch (Ashall et al. 2014; Kawabata et al. 2014; Marion et al. 2015).

For the LVG group SN 2011fe (Parrent et al. 2012; Graham et al. 2015), the blueshifted nebular [Fe II] λ7155 and [Ni II] λ7378 emission fits well into the model of Maeda et al. (2010a, see also McClelland et al. 2013). SN 2011fe also had notably lower $v_{\rm SiII}$ than SN 2014J around B-band maximum (Parrent et al. 2012; Goobar et al. 2014).

4.3. The 7210 Å feature in the spectra of SN 2011fe and 2014J

As indicated in Fig. 4, there appears to be a spectral feature around the observed wavelength 7210 Å for both SN 2011fe and 2014J, with a width roughly like the one expected from a single spectral line from ablated gas. Had this feature coincided with the expected wavelength of Hα, for example, the flux of the feature would have corresponded to a level greater than the 3σ statistical limit of the Hα flux in Fig. 3, and could have mistakenly been taken as evidence of ablated gas. This shows the importance of making a sanity check as in Sect. 3.3 and not just relying on statistical errors to set upper limits on spectral line fluxes. The question arises as to whether the feature is due to any clumpiness or asymmetry in the supernova ejecta, to ablated gas from a companion, to some other source, or to an observational artefact. This feature is seen in all four individual frames for SN 2014J and appears in both SNe. From an inspection of Fig. 1, it appears to be the only one of its sort, except perhaps for a feature at 7155 Å in the SN 2014J spectrum. The spectra of SN 2011fe at 329 days by Graham et al. (2015) and at 331 days by Taubenberger et al. (2015) have, unfortunately, signal-to-noise ratios that are too low to support or reject the tentative feature at 7210 Å for that SN.

We used The Atomic Line List V2.05B18[3] to search for possible spectral lines that could explain the 7210 Å feature of both SNe in Fig. 4, but find no obvious counterpart other than those most likely responsible for the main peaks, i.e., the usual suspects of forbidden lines of Fe and Ni (e.g., McClelland et al. 2013). Neither do we find any other obvious candidate for the 7155 Å feature. We have also looked at late spectra of SNe 1998bu, 2000cx, 2001el, and 2005cf (cf. Fig. 5 for references discussing these spectra), but do not find a similar feature for those SNe. This could partly be due to lower signal-to-noise in the spectra of these SNe. In any case, there is no support for a 7210 Å feature in their spectra.

The 7155 Å and 7210 Å features occur in a spectral region with telluric molecular absorption, which can also be traced in the standard stars used during the LBT and NOT runs. The most likely explanation for the features is that they are therefore observational artefacts from this absorption.

4.4. Implications for SNe 1998bu, 2000cx, 2001el, 2005am, and 2005cf

Apart from SNe 2011fe and 2014J, Fig. 5 shows upper limits on hydrogen-rich ablated gas for the five previous SNe Ia for which there are upper limits on Hα in late spectra. These limits are all lower than in the models of Liu et al. (2012) and are also close to the lowest mass of hydrogen-rich ablated gas in the models of Pan et al. (2012). No estimated limits on helium-rich ablated gas exist for these SNe. Possible progenitor models for these five SNe could therefore be helium-rich donor systems, DD systems, spun-up/spun-down super-Chandrasekhar WD progenitors, or perhaps hydrogen-rich donor systems with a large separation between the WD and the non-degenerate companion, where the latter is likely to be a main-sequence star as donor (cf. the models of Pan et al. 2012). The only systems fully ruled out are those with red giant donors and those with close main-sequence donors. According to Fig. 12 of Pan et al. (2012), main-sequence donor systems with a separation of $\lesssim 6\,R_\star$ are ruled out for SNe 2005am and 2005cf, as well as $\lesssim 4.5\,R_\star$ for SNe 1998bu, 2000cx, 2001el.

There are limited constraints on the progenitor systems of these supernovae from other investigations. For example, narrow emission lines were looked for in spectra of SNe 2000cx and 2001el, but no such emission was detected (Mattila et al. 2005; Lundqvist et al. 2013), and SN 2000cx showed no time-varying narrow interstellar/circumstellar absorption features (Patat et al. 2007a). SN 1998bu had a light echo (Cappellaro et al. 2001; Garnavich et al. 2001), but that was due to foreground material and not to a CSM. SN 2005cf was observed early in the ultraviolet (UV) with the HST (Wang et al. 2012) and with *Swift*, starting −8.8 and −7.8 days before B maximum, respectively. A comprehensive compilation of data and an analysis were presented in Gall et al. (2012), but there is no evidence of enhanced early flux indicative of the ejecta interacting with nearby material. *Swift* also observed SN 2005am in the UV from −1 day and onwards (Bufano et al. 2009), but nothing conspicuous with regard to the nature of the progenitor system was detected.

[3] http://www.pa.uky.edu/~peter/newpage/

Amongst all these SNe, SN 2000cx is clearly the oddball. Although it shares some properties with the overluminous SN 1991T, it is different enough to form a separate category that includes SN 2013bh (Silverman et al. 2013). It probably stems from an old, low-metallicity population, which together with its spectral evolution, indicate a DD or a SD delayed detonation scenario (Silverman et al. 2013, and references therein). Since a helium-star donor system is likely to originate in relatively massive progenitors, Wang et al. (2009) estimate that the maximum delay time for these SNe is $\sim 10^8$ yr. This probably rules out a similar progenitor for SN 2000cx.

4.5. Uncertainties

In our models we have used the W7 model (Nomoto et al. 1984), which produces 0.6 $M_\odot$ of ^{56}Ni. The excitation of the ablated gas depends on the exact amount of ^{56}Ni, as well as on the distributions of the nickel and the ablated gas. It also depends on where the positrons deposit their energy. As discussed in Sollerman et al. (2004), we have assumed local and instantaneous deposition of the positron energy. Neither microscopic nor macroscopic mixing of the ablated gas into the supernova ejecta was done. How all this is included and treated in our models affects the predicted fluxes of the lines we discuss. However, none of these uncertainties should translate into dramatic changes in the modelled line emission.

Of potentially greater importance is that the number of elements and atomic levels in our models are somewhat limited (cf. Sollerman et al. 2004, and references therein). This could lead us to underestimate line scattering and fluorescence. As noted in Pérez-Torres et al. (2014), more recent models (e.g., Jerkstrand et al. 2011) with more extensive line lists and more complete sets of ions and atomic levels, albeit not yet time-dependent, should be used to estimate these effects.

As we have pointed out, the amount of ablated gas, or rather the gas lost by a SD companion at velocities $\lesssim 10^3$ km s^{-1} after impact, differs between models from different research groups. This is highlighted by Fig. 5. More such modelling is warranted, especially for the fairly restricted range of possible progenitor systems of SNe 2011fe and 2014J (cf. Sect. 4.1). As an important boundary condition for possible SD progenitor systems, one must consider the strengthened evidence of a fairly long (10^8 yrs) minimum delay time for SNe Ia in general (e.g., Anderson et al. 2015). This could prove hazardous for the helium-star donor channel since the maximum delay time for such systems could be $\sim 10^8$ yrs (Wang et al. 2009). Refined binary evolution models are needed to see whether this channel is likely to produce a noticeable fraction of SNe Ia.

There is also uncertainty in our results owing to the adopted distance and reddening to the supernovae. According to NED[4], the uncertainty in distance to SN 2011fe is ~6%, and for modern measurements to M82 (for SN 2014J) it is ~9%. If we assign 10% as an uncertainty for the distance in general, this transforms into ~20% in estimated values for the ablated mass. For SN 2011fe, uncertainties due to reddening are not an issue, whereas for SN 2014J the reddening is significant. There is good knowledge about the absolute luminosity so the reddening is well established (Amanullah et al. 2014). The combined effect of distance and reddening is estimated to cause an uncertainty in the ablated mass of ~30% for SN 2014J. This is significant, but less than the uncertainties in our modelling.

[4] http://ned.ipac.caltech.edu

5. Conclusions and outlook

We observed SN 2014J with NOT/ALFOSC 315 days after the explosion, and also used an archival spectrum of SN 2011fe 294 days past explosion (presented in Shappee et al. 2013) to see if there is any trace of ablated gas from a SD companion. Guided by our modelling in Lundqvist et al. (2013), we concentrated on possible emission in Hα, [O I] λ6300 or [Ca II] $\lambda\lambda$7291, 7324. We found no such emission, and from that we derived statistical upper limits on the mass of hydrogen-rich gas. These limits were, however, shown to be overwhelmed by systematic effects. When the latter are included, the limits on hydrogen-rich ablated gas are 0.003 $M_\odot$ and 0.0085 $M_\odot$ for SNe 2011fe and 2014J, respectively, where the limit for SN 2011fe should supersede that of Shappee et al. (2013), and the one for SN 2014J is the second lowest ever. Assuming that the O/He and Ca/He ratios and the efficiency of line emission are the same for helium-dominated ablated gas and for hydrogen-rich gas, we derived upper limits on the mass of helium-rich ablated gas. In this case, [O I] λ6300 provides the most stringent upper limits on the ablated gas, which are 0.002 $M_\odot$ and 0.005 $M_\odot$ for SNe 2011fe and 2014J, respectively.

These upper limits were compared with the most recent models which have predicted the amount of stripped and ablated gas (Liu et al. 2012, 2013b; Pan et al. 2012). For hydrogen-rich donors, our results are incompatible with red giants and with main-sequence donors if the separation between the binary companions are $\lesssim 6\ R_\star$ for SN 2014J and $\lesssim 8.5\ R_\star$ for SN 2011fe, where $R_\star = 5.51 \times 10^{10}$ cm is the radius of the main-sequence companion in the models of Pan et al. (2012). Also, most helium-rich donors are ruled out, except for those with the largest separation. Using the models of Pan et al. (2012), helium-rich donors with a separation of $\lesssim 8{\times}10^{10}$ cm and $\lesssim 6{\times}10^{10}$ cm from the white dwarf are ruled out for SNe 2011fe and 2014J, respectively.

When we combined these results with findings from pre-explosion imaging and very early observations that constrain possible interactions with a companion, accretion disk, or a CSM, then essentially all hydrogen-rich main-sequence donor systems could be ruled out for SN 2011fe, while we cannot state this for SN 2014J. For both supernovae, our results have so far been the most constraining for helium-rich donors. Helium-rich donor systems may, however, have other problems, since the likely modelled delay time of such systems is $\lesssim 10^8$ yr (Wang et al. 2009), at the same time as recent observational findings of SNe Ia show a general delay time of $\gtrsim 10^8$ yr (Anderson et al. 2015), leaving only a low probability that these systems are progenitors of SNe Ia in general. Some support for a SD origin of SN 2014J could come from very early observations showing enhanced emission compared to the expected one (Goobar et al. 2015) for an isolated exploding white dwarf, as well as the early emergence of gamma-ray line emission (Diehl et al. 2014). According to our findings, the tentative non-degenerate companion would have to be well separated from the WD. Other possible progenitor systems for SNe 2011fe and 2014J are SD systems with a spun-up/spun-down super-Chandrasekhar white dwarf or DD systems. Continued radio monitoring of the SNe may reveal whether any of these systems are possible (Pérez-Torres et al. 2014).

Data for SNe 1998bu, 2000cx, 2001el, 2005am, and 2005cf were used to constrain their origins. Possible progenitor models for these SNe are found to be helium-rich donor systems, DD systems, spun-up/spun-down super-Chandrasekhar WD progenitors, or perhaps systems with a main-sequence star as donor, provided they are well separated from the white dwarfs.

However, as for SNe 2011fe and 2014J, helium-rich donors could be rather unlikely owing to their short delay times, and is probably excluded for SN 2000cx owing to the nature of its host galaxy.

For the broad lines of SNe 2011fe and 2014J, it was found that the [Ni II] λ7378 emission is redshifted by $\sim$+1300 km s^{-1}, as opposed to a blueshift of $\sim$−1100 km s^{-1} for SN 2011fe. Also, [Fe II] λ7155 appears to be redshifted for SN 2014J, and it has distinct substructures. Broad lines at shorter wavelengths, which are dominated by [Co III] line emission, do not show any velocity shifts between SNe 2011fe and 2014J. This fits nicely into the model of Maeda et al. (2010b), where low-ionisation lines are expected from asymmetrically distributed matter in the centre, whereas higher-ionisation lines originate further out where spherical symmetry is more likely. Both SNe 2011fe and 2014J have a slow decline rate for the velocity of the Si II λ6355 absorption trough just after *B*-band maximum. SN 2011fe fits well into the general picture that such SNe have blueshifted nebular emission, while SN 2014J belongs to a minority that instead has redshifted nebular emission. SN 2014J also has a higher velocity ($\approx$11 750 km s^{-1}) of this trough at *B*-band maximum than usual.

Although we cannot count on being blessed with several very nearby SNe Ia such as SNe 2011fe and 2014J in the near future, late spectra have now been obtained for more than just a handful of SNe. As shown in Fig. 5, useful constraints on progenitor systems can also be put on SNe Ia at 20–30 Mpc using our method. Concerted multi-wavelength efforts should be able to narrow down possible progenitor systems of SNe Ia. Very early observations are needed to constrain or detect possible interaction with a binary or circumstellar gas. Late observations in the optical and infrared are both needed to constrain emission from ablated gas, and in the radio to map circumstellar and interstellar gas. On the modelling side, we encourage detailed radiative transfer calculations, with longer line lists than used by us, to either confirm or reject our limits on the ablated gas.

Acknowledgements. Based on observations made with the Nordic Optical Telescope, operated by the Nordic Optical Telescope Scientific Association at the Observatorio del Roque de los Muchachos, La Palma, Spain, of the Instituto de Astrofisica de Canarias. We thank Jussi Harmanen, Tapio Pursimo, and Ditte Slumstrup for doing the spectroscopic observations at the NOT, and Rahman Amanullah for discussions. P.L. acknowledges support from the Swedish Research Council. This research made use of the NASA/IPAC Extragalactic Database (NED), which is operated by the Jet Propulsion Laboratory, California Institute of Technology, under contract with the National Aeronautics and Space Administration.

References

Amanullah, R., Goobar, A., Johansson, J., et al. 2014, ApJ, 788, L21
Anders, E., & Grevesse, N. 1989, Geochim. Cosmochim. Acta, 53, 197
Anderson, J. P., James, P. A., Förster, F., et al. 2015, MNRAS, 448, 732
Ashall, C., Mazzali, P., Bersier, D., et al. 2014, MNRAS, 445, 4424
Benetti, S., Cappellaro, E., Mazzali, P. A., et al. 2005, ApJ, 623, 1011
Bloom, J. S., Kasen, D., Shen, K. J., et al. 2012, ApJ, 744, L17
Brown, P. J., Dawson, K. S., de Pasquale, M., et al. 2012, ApJ, 753, 22
Bufano, F., Immler, S., Turatto, M., et al. 2009, ApJ, 700, 1456
Cappellaro, E., Patat, F., Mazzali, P. A., et al. 2001, ApJ, 549, L215
Chandler, C. J., & Marvil, J. 2014, ATel, 5812
Chomiuk, L., Soderberg, A. M., Moe, M., et al. 2012, ApJ, 750, 164
de Vaucouleurs, G., de Vaucouleurs, A., Corwin, H. G., Jr., et al. 1991, Third Reference Catalogue of Bright Galaxies (New York: Springer)
Diehl, R., Siegert, T., Hillebrandt, W., et al. 2014, Science, 345, 1162
Dilday, B., Howell, D. A., Cenko, S. B., et al. 2012, Science, 337, 942
Di Stefano, R., Voss, R., & Clayes, J. S. W. 2011, ApJ, 738, L1
Foley, R. J., Fox, O. D., McCully, C., et al. 2014, MNRAS, 443, 2887
Gall, E. E. E., Taubenberger, S., Kromer, M. 2012, MNRAS, 427, 994
Garnavich, P. M., Kirshner, R. P., Challis, P., et al. 2001, BAAS, 33, 1370
Goobar, A., & Leibundgut, B. 2011, Ann. Rev. Nucl. Part. Sci., 61, 251
Goobar, A., Johansson, J., Amanullah, R., et al. 2014, ApJ, 784, L12
Goobar, A., Kromer, M., Siverd, R., et al. 2015, ApJ, 799, 106
Graham, M. L., Valenti, S., Fulton, B. J., et al. 2014, ApJ, submitted [arXiv:1412.0653]
Graham, M. L., Foley, W., Zheng, W., et al. 2015, MNRAS, 446, 2073
Hachisu, I., Kato, M., Saio, H., & Nomoto, K. 2012, ApJ, 744, 69
Hancock, P. J., Gaensler, B. M., & Murphy, T. 2011, ApJ, 735, 35
Horesh, A., Kulkarni, S. R., Fox, D. B., et al. 2012, ApJ, 746, 21
Hughes, J. P., Chugai, N., Chevalier, R., Lundqvist, P., & Schlegel, E. 2007, ApJ, 670, 1260
Iben, Jr., I., & Tutukov, A. V. 1984, ApJS, 54, 335
Ivanova, N., & Taam, R. E. 2004, ApJ, 601, 1058
Jerkstrand, A., Fransson, C., & Kozma, C. 2011, A&A, 535, A45
Johansson, J., Goobar, A., Kasliwal, M. M., et al. 2014, MNRAS, submitted [arXiv:1411.3322]
Justham, S. 2011, ApJ, 730, L34
Kasen, D. 2010, ApJ, 708, 1025
Kawabata, K. S., Akitaya, H., Yamanaka, M., et al. 2014, ApJ, 795, L4
Kelly, P. L., Fox, O. D., Filippenko, A. V., et al. 2014, ApJ, 790, 3
Kozma, C., Fransson, C., Hillebrandt, W., et al. 2005, A&A, 437, 983
Leonard, D. C. 2007, ApJ, 670, 1275
Levanon, N., Soker, N., & García-Berro, E. 2015, MNRAS, 447, 2803
Li, W., Bloom, J. S., Podsiadlowski, P., et al. 2011, Nature, 480, 348
Liu, Z. W., Pakmor, R., Röpke, F. K., et al. 2012, A&A, 548, A2
Liu, Z. W., Kromer, M., Fink, M., et al. 2013a, ApJ, 778, 121
Liu, Z. W., Pakmor, R., Seitenzahl, I. R., et al. 2013b, ApJ, 774, 37
Lundqvist, P., Mattila, S., Sollerman, J., et al. 2013, MNRAS, 435, 329
Maeda, K., Benetti, S., Stritzinger, M., et al. 2010a, Nature, 466, 82
Maeda, K., Taubenberger, S., Sollerman, J., et al. 2010b, ApJ, 708, 1703
Maeda, K., Kutsuna, M., & Shigeyama, T. 2014, ApJ, 794, 37
Maoz, D., Mannucci, F., & Nelemans, G. 2014, ARA&A, 52, 107
Margutti, R., Soderberg, A. M., Chomiuk, L., et al. 2012, ApJ, 751, 134
Margutti, R., Parrent, J., Kamble, A., et al. 2014, ApJ, 790, 52
Marietta, E., Burrows, A., & Fryxell, B. 2000, ApJS, 128, 615
Marion, G. H., Sand, D. J., Hsiao, E. Y., et al. 2015, ApJ, 798, 39
Mattila, S., Lundqvist, P., Sollerman, J., et al. 2005, A&A, 443, 649
McClelland, C. M., Garnavich, P. M., Milne, P. A., Shappee, B. J., & Pogge, R. W. 2013, ApJ, 767, 119
Minkowski, R. 1939, ApJ, 89, 156
Munari, U., Henden, A., Belligoli, R., et al. 2013, New Astron., 20, 30
Nomoto, K. 1982, ApJ, 253, 798
Nomoto, K., Thielemann, F.-K., & Yokoi, K. 1984, ApJ, 286, 644
Nugent, P. E., Sullivan, M., Cenko, S. B., et al. 2011, Nature, 480, 344
Pakmor, R., Röpke, F. K., Weiss, A., & Hillebrandt, W. 2008, A&A, 489, 983
Pan, K.-C., Ricker, P. M., & Taam, R. E. 2012, ApJ, 750, 151
Panagia, N., Van Dyk, S. D., Weiler, K. W., et al. 2006, ApJ, 646, 369
Parrent J. T., Howell, D. A., Friesen, B., et al. 2012, ApJ, 752, L26
Patat, N., Benetti, S., Justham, S., et al. 2007a, A&A, 474, 931
Patat, N., Chandra, P., Chevalier, R., et al. 2007b, Science, 317, 924
Pérez-Torres, M. A., Lundqvist, P., Beswick, R. J., et al. 2014, ApJ, 792, 38
Perlmutter, S., Aldering, G., Goldhaber, G., et al. 1999, ApJ, 517, 565
Pogge, R. W., Atwood, B., Brewer, D. F., et al. 2010, Proc. SPIE, 7735, 77350
Press, W. H., Teukolsky, S. A., Vetterling, W. T., & Flannery, B. P. 1992, Numerical Recipes in C. The Art of Scientific Computing, 2nd edn. (Cambridge: Cambridge Univ. Press)
Riess, A., Filippenko, A. V., Challis, P., et al. 1998, AJ, 116, 1009
Rice, J. A. 2007, Mathematical Statistics and Data Analysis 3rd edn. (Duxbury, Thomson Brooks/Cole)
Russell, B. R., & Immler, S. 2012, ApJ, 748, L29
Shappee, B. J., Stanek, K. Z., Pogge, R. W., & Garnavich, P. M. 2013, ApJ, 762, L5
Shen, K. J., Guillochon, J., & Foley, R. J. 2013, ApJ, 770, L35
Silverman, J. M., Vinko, J., Kasliwal, M. M., et al. 2013, MNRAS, 436, 1225
Simon, J. D., Gal-Yam, A., Gnat, O., et al. 2009, ApJ, 702, 1157
Soker, N. 2015, MNRAS, submitted, ArXiv e-prints [arXiv:1501.07729]
Sollerman, J., Lindahl, J., Kozma, C., et al. 2004, A&A, 428, 555
Sternberg, A., Gal-Yam, A., Simon, J. D., et al. 2014, MNRAS, 443, 1849
Taubenberger, S., Kromer, M., Pakmor, R., et al. 2013, ApJ, 775, L43
Taubenberger, S., Elias-Rosa, N., Kerzendorf, W. E., et al. 2015, MNRAS, 448, 48
Thielemann, F.-K., Nomoto, K., & Yokoi, K. 1986, A&A, 158, 17
Torres, G. 2010, AJ, 140, 1158
Wang, B., Meng, X., Chen, X., & Han, Z. 2009, MNRAS, 395, 847
Wang, X., Wang, L., Filippenko, A., et al. 2012, ApJ, 749, 126
Webbink, R. F. 1984, ApJ, 277, 355
Whelan, J., & Iben, I. J. 1973, ApJ, 186, 1007
Zheng, W., Shivvers, I., Filippenko, A. V., et al. 2014, ApJ, 783, L24